

Elastic properties of charge-density-wave conductors in applied electric fields

L. C. Bourne and A. Zettl

Department of Physics, University of California, Berkeley, Berkeley, California 94720

(Received 24 February 1987)

The elastic properties of the charge-density-wave (CDW) conductors TaS₃ and NbSe₃ have been measured in the presence of ac, dc, and combined ac and dc longitudinal electric fields. For both TaS₃ and NbSe₃, application of ac fields E_{ac} in the MHz frequency range softens the crystal lattice (as indicated by a decrease in Young's modulus Y), even for values of E_{ac} well below the dc threshold field E_T for CDW depinning. For applied dc fields E_{dc} , lattice softening is observed only for $E_{dc} > E_T$, consistent with previous studies. For combined ac and dc fields, anomalies in the electronic response (such as Shapiro step structure) are reflected also in Y and the internal friction δ . On mode-locked steps, the elastic constants tend toward their pinned CDW values, despite the finite CDW drift velocity. It is suggested that these electroelastic experiments probe directly the internal degrees of freedom of the CDW, and our results are discussed in terms of applicable theoretical models.

I. INTRODUCTION

There has been much recent experimental and theoretical interest in the charge-density-wave (CDW) state associated with a growing class of low-dimensionality electronic materials.¹ The CDW is characterized by a macroscopic occupation of $2k_F$ phonons, a corresponding modulation of the electronic charge density, and a gap in the single-particle excitation spectrum. In many cases of interest (such as NbSe₃, TaS₃, and K_{0.3}MoO₃), the CDW conductor is metallic (but anisotropic) at room temperature, with a moderately high (order 100 K) Peierls transition temperature T_p to the CDW state. Below T_p the (single-particle) transport often resembles that of a narrow-band semiconductor.

A particularly useful probe for studying *static* CDW properties has been elastic measurements. Early "vibrating reed" studies² on quasi-two-dimensional CDW materials such as NbSe₂ and TaSe₂ showed sharp anomalies in Young's modulus Y and internal friction δ at the structural CDW transitions; such measurements can and have been related³ to thermodynamic properties such as specific heat, thermal expansion, and stress dependence of T_p . Since the first observation of nonlinear conduction in the CDW compound NbSe₃, much attention has been focused on the unusual transport properties of the CDW condensate.¹ Materials such as NbSe₃, TaS₃, (TaSe₄)₂I, and K_{0.3}MoO₃ display enhanced dc conductivity for dc electric fields E_{dc} exceeding a well-defined threshold field E_T (corresponding to a depinning and subsequent sliding of the CDW), frequency-dependent ac conductivity in the MHz frequency range (corresponding to polarization of the CDW about pinning centers), and coherent current oscillations (narrow-band noise) for $E_{dc} > E_T$. Mixing between the internally generated narrow-band noise and an externally applied ac electric field can also lead to electronic interference structure in the current-voltage (I - V) characteristics of the crystal, and mode-locked states.

The same elastic measurement methods developed for static CDW systems are well suited to the study of CDW *dynamics*. Brill and Roark⁴ first showed that both Y and δ in TaS₃ are strongly affected by applied dc fields $E_{dc} > E_T$. In general, dc field-induced depinning of the CDW causes the crystal lattice to soften and the internal friction to increase. Similar field dependences were obtained by Mozurkewich *et al.*⁵ for NbSe₃ and (TaSe₄)₂I. A detailed account of low-frequency elastic properties of TaS₃ for applied dc electric fields is given in Ref. 6. CDW depinning in TaS₃ has also been studied by conventional ultrasonic techniques adapted to the long thin crystal geometry.⁷

In this report we discuss measurements of the elastic properties (Y and δ) of TaS₃ (orthorhombic phase) and NbSe₃, in the presence of externally applied ac, dc, and combined ac+dc electric fields. The elastic properties are found to be sensitive to CDW motion, even in the limit where the CDW is excited by a very low amplitude ac field $E_{ac} < E_T$. For applied dc fields E_{dc} , lattice softening is observed for $E_{dc} > E_T$, consistent with previous studies.⁴⁻⁶ In the presence of combined ac+dc fields, a strong correspondence between the electronic response of the CDW (as determined by differential resistance measurements) and the elastic response is observed. Our results suggest an important role played by internal degrees of freedom of the CDW condensate.

This paper is organized as follows: In Sec. II we describe the measurement technique and experimental results. Section III presents applicable theoretical models and a discussion of our experimental results in terms of these models. This is followed by a conclusion in Sec. IV. Some of our experimental results have been previously published.⁸

II. EXPERIMENTS AND RESULTS

Materials used in this study consisted of single crystal samples of NbSe₃ and orthorhombic TaS₃, synthesized by conventional vapor transport methods. dc I - V

tively the amplitude and Q measured with zero applied external field. In single sweep data recordings, our experimental method was typically sensitive to relative changes in Y of order 10^{-4} , and absolute changes in δ also of order 10^{-4} ; with signal averaging the sensitivity of both parameters could be improved by at least 1 order of magnitude.

A. TaS₃

Figure 2 shows, for a TaS₃ crystal at $T=152$ K, Y , δ , and dV/dI as measured in the presence of an externally applied longitudinal ac field $E_{ac} \cos(\omega_{ex}t)$ with $\omega_{ex}/2\pi=1$ MHz. No dc bias is present. The horizontal amplitude scale has been normalized to the dc conductivity threshold field E_T , measured in the absence of any ac excitation. From Fig. 2 it is clear that an ac field of moderate amplitude has a significant effect on both Y and δ ; dV/dI is far less sensitive, and begins to deviate from its $E_{ac}=0$ value only above approximately $E_{ac}/E_T=5$. The observed decrease in Y and increase in δ with increasing E_{ac} indicates that the external ac field tends to soften the crystal lattice while increasing the internal friction. Both parameters are here measured on time scales much longer than ω_{ex}^{-1} .

From Fig. 2 it is difficult to see clearly if Y and δ deviate from their zero-field values for E_{ac} finite but less than E_T . Figure 3 shows this parameter range in detail, again for TaS₃. Even for $E_{ac}/E_T < 1$, Y is seen to decrease smoothly with increasing E_{ac} , with no evidence for any threshold behavior. Assuming simple classical dynamics for the CDW, we would expect the CDW to remain always pinned for $E_{ac}/E_T < 1$, independent of damping. We therefore identify the lattice softening of Fig. 3 with

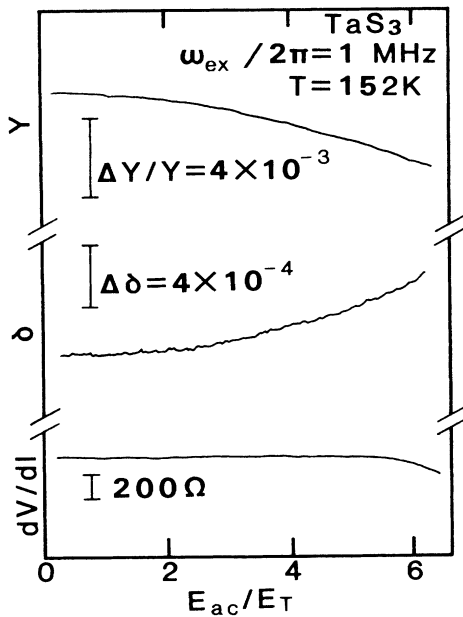


FIG. 2. Y , δ , and dV/dI in TaS₃ as functions of ac field amplitude E_{ac} . The crystal lattice softens and internal friction increases with increasing E_{ac} . No dc bias field is present (sample TaS₃ number 32: $R=2.9$ k Ω , $I_T=63$ μ A, length equals 1.5 mm).

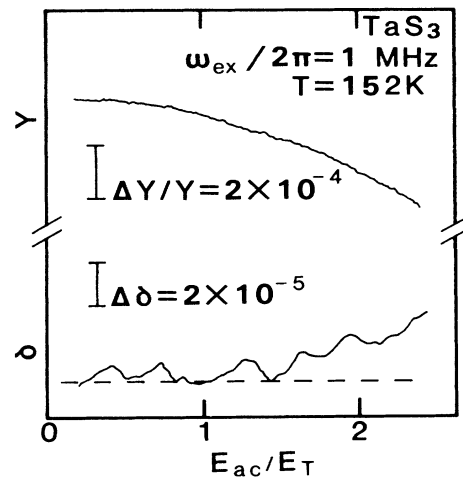


FIG. 3. Detailed behavior of Y and δ as functions of E_{ac} in TaS₃. Lattice softening occurs even for E_{ac} much smaller than the dc threshold field E_T (sample TaS₃ number 32).

excitation of the pinned phason mode, not the sliding Fröhlich mode. Figure 3 also shows the internal friction δ . The vertical scale has been greatly expanded, and the fine structure observed is entirely due to instrumental drifts. The dashed line represents the averaged $E_{ac}=0$ value. For $E_{ac}/E_T < 1$, we find, within experimental resolution, no change in δ ; for $E_{ac}/E_T=2$, however, δ has increased significantly, with $\Delta\delta=2 \times 10^{-5}$.

The lattice softening observed in Figs. 2 and 3 is strongly frequency (ω_{ex}) dependent. Figure 4 shows, for a TaS₃ crystal at $T=151$ K, the relative change in Y with increasing E_{ac} measured for three different values of ω_{ex} . As with the data of Figs. 2 and 3, Fig. 4 was obtained with $E_{dc}=0$. Figure 4 shows that the ac field-induced lattice softening effect is only observed for relatively low values of ω_{ex} . Curve A, for example, which corresponds

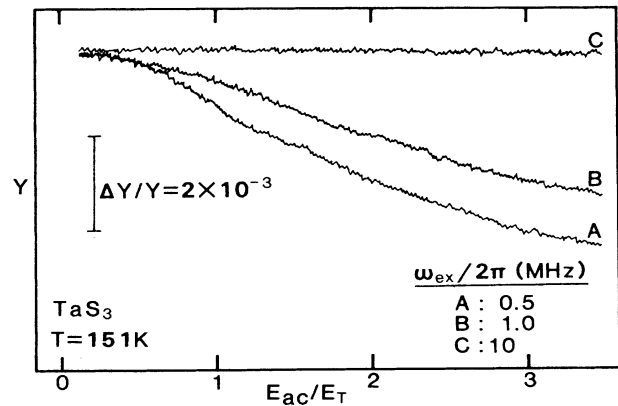


FIG. 4. Y as a function of E_{ac} in TaS₃, for three different values of ac frequency ω_{ex} (sample TaS₃ number 31: $R=3.8$ k Ω , $I_T=75$ μ A, length equals 0.8 mm).

to $\omega_{\text{ex}}/2\pi=0.5$ MHz, shows a relative change in Y of order 10^{-3} at $E_{\text{ac}}/E_T=1$, while curve C, corresponding to $\omega_{\text{ex}}/2\pi=10$ MHz, shows no change in Y even for $E_{\text{ac}}/E_T > 3$.

A vertical cut through data similar to that presented in Fig. 4 is shown in Fig. 5, where the relative change in Y is plotted as a function of ω_{ex} , for fixed $E_{\text{ac}}/E_T=2.6$. Over a limited range in frequency, $\Delta Y/Y$ changes linearly with frequency, while as $\omega_{\text{ex}} \rightarrow 0$ $\Delta Y/Y$ asymptotically approaches the dc limit (measured independently with an applied dc field $E_{\text{dc}}/E_T=2.6$). At high values of ω_{ex} , Y approaches the zero bias limit.

Behavior similar to that shown in Fig. 5 was obtained in TaS₃ for other fixed values of $E_{\text{ac}}/E_T \gg 1$. For $E_{\text{ac}}/E_T \approx 1$, however, the behavior of Y is strikingly different. Figure 6 shows $\Delta Y/Y$ versus ω_{ex} for $E_{\text{ac}}/E_T=1$. The dashed line is a guide to the eye drawn through the few accurately determined data points. From Fig. 6 it appears that $\Delta Y/Y$ deviates dramatically and smoothly from zero as the frequency is lowered from 10 MHz, yet the $\omega_{\text{ex}}=0$ (dc) point is clearly at $\Delta Y/Y=0$. As we discuss later, this behavior may suggest critical behavior in Y as ω_{ex} approaches a characteristic frequency ω_{cr} .

We now consider the effect of combined ac and dc electric fields on Y and δ . Figure 7 shows Y , δ , and dV/dI for a TaS₃ crystal at $T=152$ K, as functions of dc bias. The dc bias is represented as a ratio of applied dc bias current I_{dc} to the dc threshold current I_T (measured with no ac field applied). The dc bias field is related to I_{dc} by $E_{\text{dc}}=I_{\text{dc}}R/l$, where R is the (nonlinear) sample resistance and l is the sample length. For all data in Fig. 7, the frequency of the applied ac field is $\omega_{\text{ex}}/2\pi=1$ MHz. Curves A in Fig. 7 are for $E_{\text{ac}}=0$; this limit corresponds to dc CDW depinning experiments performed previously on TaS₃ and other CDW conductors.⁴⁻⁷ In the bottom group of traces in Fig. 7, curve A is a conventional dV/dI versus dc bias plot. The sharp break in the curve at $I_{\text{dc}}/I_T=1$ clearly identifies the dc threshold for CDW depinning. As seen in the upper sets of traces labeled A in Fig. 7, similar breaks in Y and δ are again observed in

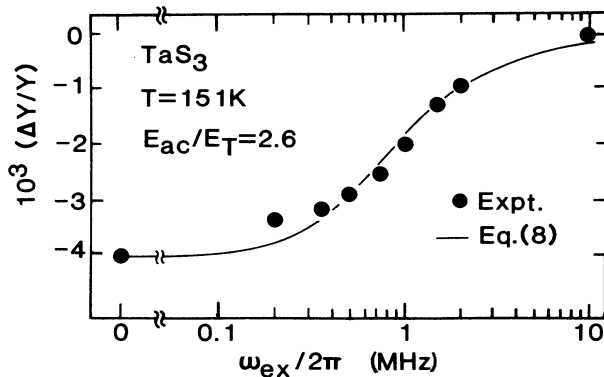


FIG. 5. $\Delta Y/Y$ as a function of ac frequency ω_{ex} in TaS₃, with E_{ac} exceeding E_T . The solid line is Eq. (8), with fitting parameters given in the text (sample TaS₃ number 31).

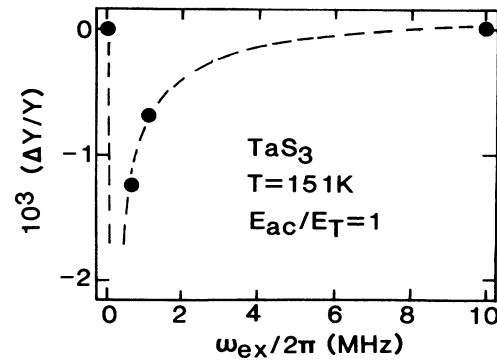


FIG. 6. $\Delta Y/Y$ as a function of ac frequency ω_{ex} in TaS₃, for $E_{\text{ac}}=E_T$. Note that $\Delta Y/Y=0$ at $\omega_{\text{ex}}=0$. The dashed line is a guide to the eye (sample TaS₃ number 31).

Y and δ at $I_{\text{dc}}/I_T=1$. For $I_{\text{dc}} > I_T$, Y decreases smoothly with increasing dc bias, and δ increases rapidly and apparently saturates near $I_{\text{dc}}/I_T=1.5$. The general features of these traces, corresponding to finite E_{dc} and zero E_{ac} , are in good agreement with previous studies.⁴⁻⁶ Curves B, C, and D in Fig. 7 show the effects of ac field on Y , δ , and dV/dI . The dV/dI traces show clearly that the break in dV/dI , i.e., the threshold for dc CDW conduction, is reduced to a lower value I_T' with the application of ac field. This electronic effect has been previously observed and studied quite extensively in TaS₃ and NbSe₃.¹¹⁻¹⁴ An important point to note is that for the dV/dI curves B and C in the lower part of Fig. 7, no change in dV/dI is observed at $I_{\text{dc}}=0$. Only when the effective depinning threshold has been reduced to zero does dV/dI at $I_{\text{dc}}=0$ become E_{ac} dependent, as is the case for curve D.

The Y and δ traces of Fig. 7 show that finite E_{ac} has a dramatic effect on the functional dependence of Y and δ on I_{dc} . It should be emphasized that in Fig. 7 the traces

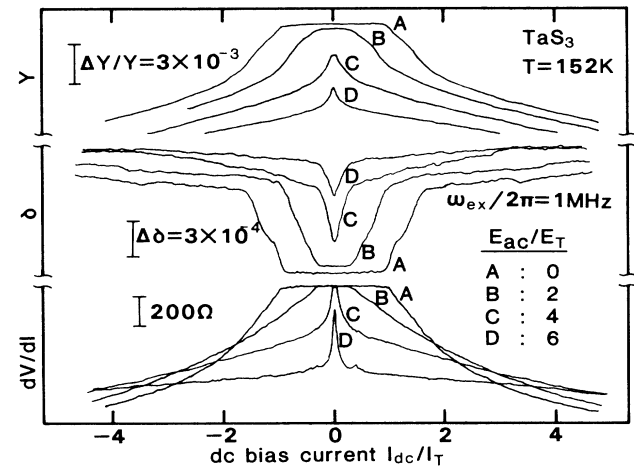


FIG. 7. Y , δ , and dV/dI as functions of dc bias in TaS₃ at $T=152$ K, for four different values of E_{ac} . Curves within each group have not been vertically displaced (sample TaS₃ number 32).

within a group have *not* been vertically offset. With $I_{dc}=0$, the E_{ac} dependence of Y and δ in Fig. 7 is consistent with the lattice softening and increasing internal friction with increasing E_{ac} previously demonstrated in Fig. 2. For increasing I_{dc} , E_{ac} -dependent breaks in Y and δ are observed; these appear to correspond to the dc depinning threshold I_T' (see below). General features of Young's modulus are a general depression in Y with increasing E_{ac} , and a weaker dependence of Y on dc bias with increasing E_{ac} . For $I_{dc}/I_T > 2$, traces of Y corresponding to different E_{ac} values appear to converge. Extrapolating the Y data of Fig. 7 to higher I_{dc} values results in a convergence point at $I_{dc}/I_T=9$. We were not able to directly verify such a convergence experimentally due to significant Joule heating of the sample at large values of I_T and E_{ac} .

The E_{ac} dependence of internal friction δ parallels that of Y . With increasing E_{ac} , δ increases, and the value of I_{dc} at which δ "saturates" (i.e., assumes a relatively flat slope) decreases with increasing E_{ac} . The absolute saturation value of δ in the saturated region appears to increase with increasing E_{ac} , although we cannot rule out the possibility that at large I_{dc} δ becomes roughly independent of E_{ac} . Indeed, curves *C* and *D* for $I_{dc}/I_T > 4$ suggest this may be the case.

As mentioned above, the initial "breaks" in the dV/dI , Y and δ versus I_{dc} curves appear correlated. Figure 8 shows this correlation in detail for another TaS₃ sample at 151 K, with $\omega_{ex}/2\pi=1$ MHz. The vertical axis represents that value of I_{dc} (normalized to I_T) at which a finite slope first appears in the dV/dI , Y , or δ versus I_{dc} curve. For $E_{ac}/E_T > 2$, there is, for all three parameters, no region of finite slope and the breaks all occur at $I_{dc}=0$. The critical value of E_{ac}/E_T above which the breaks all occur at $I_{dc}=0$ (i.e., the critical value of E_{ac}/E_T for which I_T' is suppressed to zero) is sample

dependent; for the TaS₃ sample of Fig. 7, for example, the critical value is $E_{ac}/E_T \approx 4$. The strong correlations observed in Fig. 8 indicate that Y and δ are very sensitive to dc motion of the CDW, even in the case where the elastic constants have already been strongly perturbed by a large amplitude ac field. In the limit $E_{ac} \rightarrow \infty$, however, Fig. 7 would suggest no additional I_{dc} dependence for either Y or δ .

The general features of the Y and δ versus E_{ac} and E_{dc} behaviors shown in Fig. 7 are, for TaS₃, very temperature dependent, and to some extent sample dependent. Figure 9 shows, for TaS₃ at $T=115$ K, data in the same format as was used for Fig. 7. The same sample was used to generate the data for Figs. 7 and 9. While the dV/dI versus I_{dc} traces in Fig. 9 are qualitatively very similar to those of Fig. 7, there are important differences in dV/dI , and in particular in Y and δ . We note first that a much larger ratio of E_{ac}/E_T is required at low temperature to reduce the dc threshold field to zero; at 115 K the ratio is three times the ratio at 152 K. However, the general form of dV/dI versus I_{dc} is relatively temperature independent in this temperature range. The low-temperature behavior of Y and δ versus I_{dc} is unusual. In curve *A* of Fig. 9, which corresponds to $E_{ac}=0$, the initial break in Y is associated with an initial *increase* in Y with increasing I_{dc} ; at higher values of I_{dc} Y again decreases strongly with increasing I_{dc} , consistent with the high-temperature behavior. With increasing E_{ac} , this "bump" structure in Y remains, but moves to lower dc bias values and decreases in magnitude. For curve *C*, corresponding to $E_{ac}/E_T=12$, the bump structure has nearly coalesced near the $I_{dc}=0$ origin, and for curve *D*, corresponding to $E_{ac}/E_T=19.2$, the anomalous feature is no longer observable.

Figure 9 shows that there are no corresponding "bump" anomalies in δ near the dc threshold I_T' ; the de-

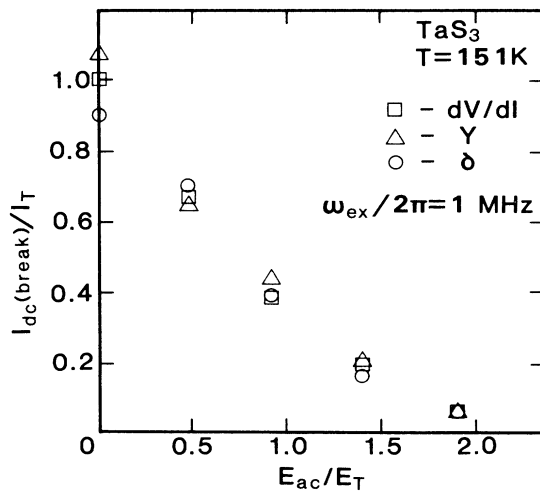


FIG. 8. Effect of an ac field on the critical dc bias for changes in dV/dI , Y , and δ . I_{dc} (break) is the dc current value at which the measured quantity begins to deviate from the $I_{dc}=0$ value. I_T is the depinning current for $E_{ac}=0$; E_T is the corresponding dc threshold field (sample TaS₃ number 31).

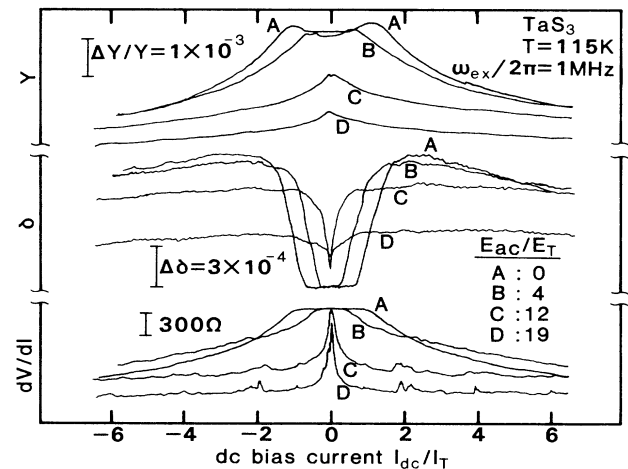


FIG. 9. Y , δ , and dV/dI as functions of dc bias in TaS₃ at $T=115$ K, for four different values of E_{ac} . The curves within each group have not been vertically displaced. This data should be compared to analogous data in Fig. 7, which is for the same TaS₃ crystal but at a higher temperature (sample TaS₃ number 32).

pinning behavior is similar to that observed at higher temperatures. At greater values of dc bias, however, Fig. 9 shows, for $E_{ac}=0$, no fast transition to a zero slope (saturated) state. Rather, curve *A* shows a broad maximum in δ near $I_{dc}/I_T=2$. At high values of E_{ac} the maximum is suppressed, and again “saturation” behavior, similar to that observed at high temperatures, results. It is important to note also that at low temperatures, the application of ac field E_{ac} causes a dramatic *decrease* in δ in the sliding CDW state; this tendency in δ is exactly opposite to that observed at high temperatures.

Although we have routinely observed the anomalous bump structure in Y and “broad maximum” structure in δ in TaS₃ at low temperatures, the features are not apparent in all crystals. We have been unable to correlate such features to other crystal parameters, for example threshold field (corresponding to sample impurity concentration) or sample size. We note that similar anomalies have been previously observed in TaS₃ at 96 K by Brill *et al.*,⁶ in the finite $E_{dc}, E_{ac}=0$ limit.

The dV/dI traces of Fig. 9 corresponding to large E_{ac} show peak structure for applied I_{dc} well beyond I_T . These peaks identify Shapiro step interference between ω_{ex} and the internal narrow-band noise frequency ω_{in} . In TaS₃ and NbSe₃, Shapiro step interference in general occurs whenever $\omega_{in}/\omega_{ex}=p/q=n$, with p and q integers.^{12,15,16} Peaks corresponding to integral values of n are denoted as harmonic interference steps, and those corresponding to nonintegral values as subharmonic steps. For a fully volume coherent crystal, Shapiro step interference can result in complete mode locking,¹⁷ where the entire CDW condensate assumes a constant drift velocity whose magnitude is dictated by ω_{ex} . During such mode locking the dc differential resistance dV/dI assumes its pinned, $E_{dc}\rightarrow 0$ value. The Shapiro step structure observed in Fig. 9 is clearly not in the fully mode-locked regime, and the interference peaks (at $I_{dc}/I_T=2$, for example) correspond to only a small portion of the CDW mode locked. Similar low-fractional locking is present in the data of Fig. 7, for example at $I_{dc}/I_T=0.3$ in dV/dI curve *D*. In neither Figs. 7 nor 9 is the experimental resolution of Y and δ sufficient to observe any corresponding structure in elastic parameters during electronic interference. Such structure does, however, exist.

Figure 10(a) shows the results of a very careful measurement of Y , δ , and dV/dI in TaS₃ at 151 K, in the presence of an ac field at $\omega_{ex}/2\pi=1$ MHz with $E_{ac}/E_T=1.3$. In the bottom dV/dI trace, Shapiro step interference is observed at $I_{dc}=55$ μ A, as identified with the vertical arrow and dashed line. This peak corresponds to $n=p/q=1/1$. Figure 10(a) shows that, corresponding to electronic Shapiro step interference in dV/dI , there occur small anomalies in Y and δ . Y shows a peak structure similar to that observed in dV/dI , while δ shows a dip during the interference. These features are seen more clearly in Fig. 10(b), which shows the detailed behavior of Y and δ in the region of the dominant Shapiro step for the same TaS₃ crystal. It is apparent that, during the electronic interference, both Y and δ tend toward their respective values assume in the *pinned* CDW state. Figure 10(b) also shows that additional Shapiro step structure

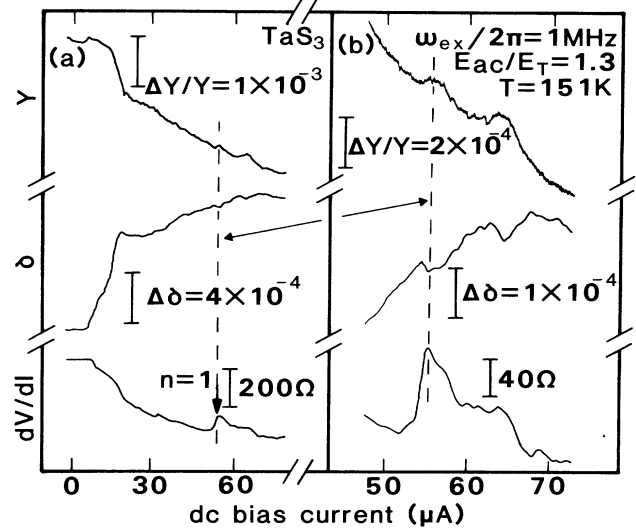


FIG. 10. Y , δ , and dV/dI in TaS₃ as functions of dc bias in the presence of an ac field. The position of the $n=1$ Shapiro step interference peak is identified with a vertical arrow. Corresponding structure is observed in Y and δ (dashed vertical line) (sample TaS₃ number 31).

in dV/dI is observed at $I_{dc}=63$ μ A. This interference peak also corresponds to $n=p/q=1/1$, and is unrelated to the peak at $I_{dc}=55$ μ A. The peak at $I_{dc}=63$ μ A apparently arises from a different portion of the sample mode locking to ω_{ex} , as can result from a nonuniform CDW current distribution in the crystal and a multivalued narrow band noise spectrum. Figure 10(b) shows that this second interference peak is again associated with well-defined anomalies in Y and δ .

B. NbSe₃

The experiments described above have in part been repeated for NbSe₃, with similar results. NbSe₃ has two CDW transitions, the first at $T_1=144$ K and the second at $T_2=59$ K. Both the upper ($T_2 < T < T_1$) and lower ($T < T_2$) CDW states are associated with pinned phason mode excitations, nonlinear Fröhlich mode conduction, narrow-band noise, and Shapiro step interference.¹ Most *electronic* experiments on NbSe₃ have been performed in the lower CDW state, where the response properties are in general more dramatic. Interestingly, the *elastic* response parameters have exactly the opposite sensitivity, with changes in the elastic properties due to the depinning of the CDW reported as being substantial in the upper CDW state but immeasurably small in the lower CDW state.⁵

Figure 11 shows Y , δ , and dV/dI as functions of dc bias current I_{dc} in the lower CDW state of NbSe₃ $T=37.9$ K. No ac field is present. The very sensitive measurement of Y and δ is associated with a large amount of instrumental noise. Nevertheless, it is apparent that the strong nonlinearity in dV/dI for $I_{dc} > I_T$ is associated with a decrease in Y and an increase in δ , similar to the behavior observed in TaS₃. For $I_{dc}/I_T=2$, there are well

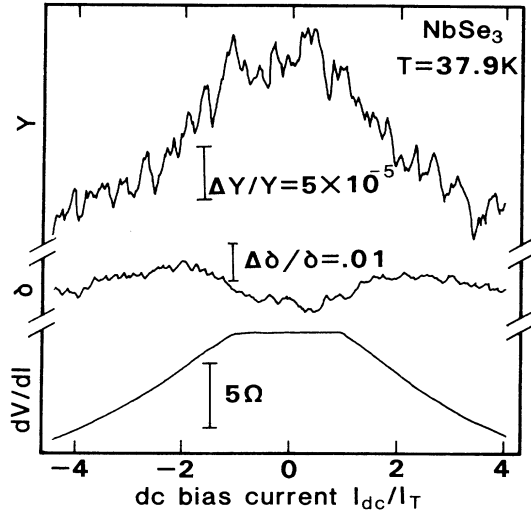


FIG. 11. Y , δ , and dV/dI as functions of dc bias in the lower CDW state of NbSe₃. (sample NbSe₃ number 38: $R = 13 \Omega$, $I_T = 68 \mu\text{A}$, length approximately equals 1 mm).

defined changes in Y of order $\Delta Y/Y = 5 \times 10^{-5}$ and in δ of order $\Delta \delta = 5 \times 10^{-3}$. There is a broad maximum in δ near $I_{dc}/I_T = 2$; for larger values of dc bias δ appears to decrease smoothly with increasing I_{dc} . No saturation in Y is observed for $I_{dc}/I_T < 5$.

Because of the relatively small changes in the elastic parameters of NbSe₃ in the lower CDW state in the presence of bias fields, we have chosen to study more carefully the elastic response in the upper CDW state. Figure 12(a) shows, Y , δ , and dV/dI as functions of dc bias current I_{dc} for NbSe₃ at $T = 135 \text{ K}$. Similar to the behavior observed in the lower CDW state, Y and δ show sharp breaks at I_T , with Y decreasing and δ increasing with increasing I_{dc} past threshold (the small increase in δ with increasing I_{dc} below I_T is due to instrumental drift). For $I_{dc}/I_T = 1.5$, δ is seen to approach a maximum and saturate. At $I_{dc}/I_T = 2$, Y shows a relative change of approximately $\Delta Y/Y = 2 \times 10^{-4}$, and $\Delta \delta = 5 \times 10^{-5}$. The change in Y is nearly an order of magnitude larger than that associated with the lower CDW state of NbSe₃. Figure 12(b) shows the additional effect of an ac field on Y , δ , and dV/dI , with $\omega_{ex}/2\pi = 2 \text{ MHz}$ and $E_{ac}/E_T = 3.8$. In the lower dV/dI trace, Shapiro step interference peaks are identified with corresponding values of n . Both harmonic and subharmonic steps are observed. The $n = 1/1$ peak is dominant and displays nearly complete mode locking. The Y and δ traces in Fig. 12(b) show that the electronic mode locking is associated with striking anomalies in Y and δ , for harmonic as well as subharmonic interference. As previously demonstrated for TaS₃, in NbSe₃ Y and δ during mode lock approach the values appropriate to the pinned CDW state. In NbSe₃ there is an approximate scaling between the degree of mode lock and the magnitude of the elastic anomalies (peak in Y and dip in δ). For example, the dominant electronic interference peak at

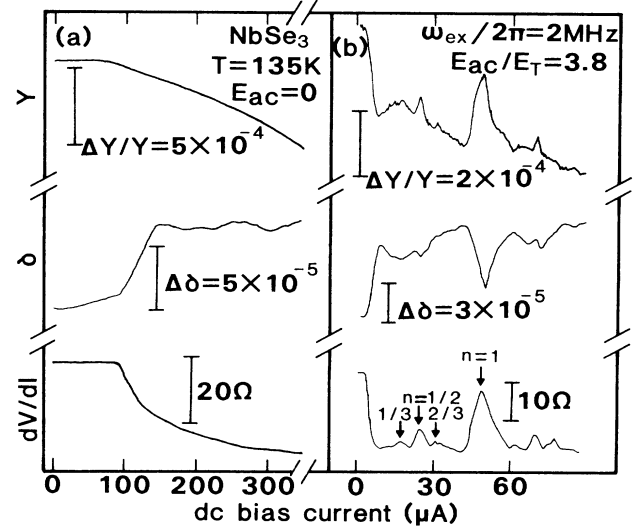


FIG. 12. Y , δ , and dV/dI as functions of dc bias in the upper CDW state of NbSe₃, (a) with $E_{ac} = 0$, and (b) with $E_{ac}/E_T = 3.8$. In (b), harmonic and subharmonic Shapiro step structure is observed in dV/dI (vertical arrows) with corresponding anomalies in Y and δ . During the electronic interference, dV/dI , Y , and δ tend toward their respective values assumed in the pinned CDW state. (a) Sample NbSe₃ number 35: $R = 220 \Omega$, $I_T = 82 \mu\text{A}$, length equals 1.1 mm. (b) Sample NbSe₃ number 33: $R = 214 \Omega$, $I_T = 100 \mu\text{A}$, length equals 1.0 mm.

$n = 1/1$ is associated with the largest anomalies in Y and δ .

III. MODELS AND DISCUSSION

CDW dynamics have been of considerable interest since the revival of Fröhlich's theory of superconductivity.¹ Models have been advanced which treat the CDW as a quantum system in which the CDW electrons coherently tunnel across an impurity pinning gap,¹⁸ or as a classical medium with¹⁹⁻²¹ or without²² internal degrees of freedom. Such models have been surprisingly successful in accounting for the electronic CDW response to applied electric fields, but in general the elastic response is not addressed.

In the absence of pinning and neglecting amplitude fluctuations, the phase ϕ of the CDW may be treated as a classical field and related to a (one-dimensional) Lagrangian²³

$$\mathcal{L} = n_1 [(m^*/2)(1/2k_F)^2(d\phi/dt)^2 - (\kappa/2)(d\phi/dx)^2], \quad (2)$$

where n_1 is the one-dimensional CDW carrier concentration, m^* is the effective mass of CDW carriers, k_F is the Fermi wave vector, and κ is a phenomenological elastic constant of the CDW given by $\kappa = \hbar v_F / 2\pi$. Including the effects of impurities and dissipation leads to an equation of motion²⁴

$$d^2\phi/dt^2 + (1/\tau)d\phi/dt + \omega_0^2 \sin(\phi) + (m/m^*)\hbar v_F^2 d^2\phi/dx^2 = 2k_F eE/m^* , \quad (3)$$

where τ is the CDW damping time, m is the electron (band) mass, ω_0 is the CDW pinning frequency, and E is the applied electric field. Assuming that the CDW phase varies only slowly in space, Eq. (3) leads to a simplified equation of motion for the collective CDW phase

$$d^2\phi/dt^2 + (1/\tau)d\phi/dt + \omega_0^2 \sin(\phi) = 2k_F \theta E/m^* \quad (4)$$

as first derived by Grüner, Zawadowski, and Chaikin.²² Equation (4) has been used extensively as a first order model to describe dc, ac, and coupled ac+dc electronic dynamics of the CDW condensate.¹² However, since the CDW is here described as a rigid particle in a rigid periodic pinning potential, all elastic effects are absent, and Eq. (4) can at best only describe the behavior of dV/dI in the presence of applied electric field; Y and δ are absent from the model.

A number of models have been advanced which specifically address elastic properties of CDW conductors. Coppersmith and Varma²⁵ have calculated the shift in longitudinal sound velocity (phonon frequency) for the underlying deformable lattice due to a sliding CDW. The predicted softening of the lattice due to CDW depinning is, however, found to be orders of magnitude smaller than that observed experimentally. Mozurkewich *et al.*⁵ have suggested that the total stiffness of a CDW crystal can be separated into contributions from the CDW condensate (Y_C) and the underlying lattice (Y_L). For a pinned CDW, the stiffnesses are additive, $Y = Y_C + Y_L$, while for a fully depinned CDW, Y_C is decoupled from the lattice, hence $Y = Y_L$. Estimated changes in Y_C/Y_L , based on the Lee-Rice²⁶ and Fukuyama-Lee²⁷ models, yield⁵ values of order 1%. The coupled phason-phonon approach thus yields elasticity anomalies within the range of experimentally observed shifts, and provides good evidence that lattice softening upon CDW depinning is indeed due to decoupling of the CDW from the underlying lattice. Littlewood²⁸ has further suggested second order contributions to Y arising from screening effects, where strain gradient terms are coupled to CDW phase gradients. In the limit of large dc bias fields, Littlewood finds a slow saturation

$$m^* d^2r/dt^2 + \gamma_c d(r-x)/dt + k_c r + eE_T \sin[2k_F(r-x)] = e[E_{dc} + E_{ac} \cos(\omega_{ext}t)] , \quad (6a)$$

$$M d^2x/dt^2 + \Gamma dx/dt + \gamma_c d(x-r)/dt + K_L x + eE_T \sin[2k_F(x-r)] = F \cos(\omega_r t) , \quad (6b)$$

where r and x are respectively the positions of the CDW center of mass and lattice, m^* is the total CDW effective mass, M_L the lattice mass, γ_c and Γ_L , respectively, the total CDW damping and internal lattice friction. k_C and K_L parametrize, respectively, the total elasticity of the CDW and underlying lattice, and $F \cos(\omega_r t)$ is the mechanical force applied to the lattice. Equations 6(a) and 6(b) have been solved in the limit of clamped-clamped boundary conditions for applied dc fields E_{dc} , ac fields $E_{ac} \cos(\omega_{ext}t)$, and combined ac+dc fields.²⁹ In the limit of finite E_{dc} , $E_{ac}=0$, Eqs. 6(a) and 6(b) predict shifts in Y due to CDW depinning consistent with experiment and in

of Y , with $\Delta Y/Y \sim (E_{dc})^{-1/2}$.

Brill *et al.*⁶ have applied standard anelastic relaxation theory to describe the detailed behaviors of Y and δ . Assuming a single relaxation time τ_0 , the frequency dependent elastic constants become

$$Y(\omega) = Y(0) + F\omega^2\tau_0^2/(1 + \omega^2\tau_0^2) \\ = Y(\infty) - F/(1 + \omega^2\tau_0^2) , \quad (5a)$$

$$\delta = F\omega\tau/(1 + \omega^2\tau_0^2) , \quad (5b)$$

where F is an (unspecified) internal variable of the system, perhaps related to temperature. By assuming constant F and a relaxation time $\tau_0 = (1.5/\omega)[E_T/(E_{dc} - E_T)]^{0.75}$, Eqs. 5(a) and 5(b) produce Y and δ versus E_{dc} curves with functional forms similar to Y and δ experimentally observed in TaS₃, but with incorrect magnitudes (experimentally, changes in Y dominate those in δ , while Eqs. 5(a) and 5(b) predict comparable shifts⁶). Brill *et al.*⁶ find that, within the anelastic relaxation model, the experiments suggest a field-dependent relaxation strength, such as $F(E_{dc}, \tau_0)$ increasing with E_{dc} for $\tau_0 \ll \omega^{-1}$. Jericho and Simson⁷ have proposed a related model, with a temperature and field-dependent relaxation strength and relaxation time, to account for high-frequency ultrasonic pulse propagation in TaS₃.

The CDW condensate and underlying lattice can be treated as coupled deformable media obeying classical mechanics.^{8,29,30} Sneddon³⁰ has considered the case of an incommensurately pinned CDW in the presence of applied dc fields E_{dc} . For $E_{dc} > E_T$, Y and δ assume forms similar to those predicted by Eqs. 5(a) and 5(b), with δ displaying a broad maximum near $E_{dc}/E_T = 2$. A sharp anomaly (peak) in Y is also found for E_{dc} near E_T . Sneddon's model suggests an important role played by internal CDW degrees of freedom in determining the behavior of δ . A related model suggested by Sherwin *et al.*^{8,29} treats the deformable CDW interacting (via an impurity pinning potential and CDW damping) with a deformable underlying lattice. In its simplest form, the equations of motion for the CDW and lattice are⁸

accord with the stiffness of the CDW condensate; the predicted increases in δ are also consistent with experiment.²⁹ The model fails in the critical region $E_{dc} = E_T^+$ where, as expected, square-root singularities dominate. In the limit of finite E_{dc} and E_{ac} , the predictions of Eqs. 6(a) and 6(b) are in agreement with lattice softening by an ac field and a recovery of lattice stiffness on mode-locked steps.²⁹ In the following discussion, we consider the importance of incorporating internal degrees of freedom of the CDW condensate in the interpretation of electroelastic CDW phenomena.

A. Finite E_{ac} , $E_{dc}=0$

Figures 2–6 clearly demonstrate that the stiffness of a TaS_3 crystal is decreased by application of an external ac electric field. The decrease is a sensitive function of the ac amplitude and frequency, with stronger effects occurring for larger ac amplitude and smaller ac frequency. For $E_{ac} > E_T$, Fig. 5 shows that ac electric fields with frequency in excess of approximately 10 MHz have no effect on Y , while at very low frequencies the dc limit of $\Delta Y/Y$ is recovered. This suggests that the lattice softening is a direct result of CDW motion (i.e., displacement). Because of the finite damping of the CDW, ac-induced displacement of the CDW from equilibrium becomes more limited at higher frequencies. Hence, at high frequencies the CDW remains strongly tied to the lattice, and Y remains large at $Y = Y_c + Y_L$. At low frequencies, the CDW displacement from the equilibrium becomes large; at sufficiently low ω_{ex} the CDW is for much of the cycle essentially depinned. In the limit $\omega_{ex} \rightarrow 0$, the dc value for $\Delta Y/Y$ of a depinned CDW is then naturally obtained, and in the limit $E_{ac} \rightarrow \infty$ we expect saturation at $Y = Y_L$.

For $E_{ac} < E_T$ the situation is similar, with $\Delta Y/Y$ becoming larger in magnitude with decreasing ω_{ex} , as observed in Fig. 6. The distinction here, when compared to the results of Fig. 5, is that as ω_{ex} tends to zero the dc limit is *not* approached smoothly, since $\Delta Y/Y = 0$ at $\omega_{ex} = 0$. This feature reflects the fact that, for $E_{ac} < E_T$, the CDW motion or displacement is zero at zero frequency.³¹

An important question is whether there exists a simple relation between $\Delta Y/Y$ and the maximum CDW displacement X_0 for a given frequency ω_{ex} . As a first approximation to the CDW displacement in the presence of E_{ac} , we neglect CDW and lattice elasticity altogether and assume the “rigid particle” motion of Eq. (4). The maximum displacement is then¹¹

$$X_0 = (eE_{ac}\omega_0^{-2}/m^*)[1 + (\omega_{ex}/\omega_0^2\tau)^2]^{1/2}. \quad (7)$$

Equation (7) has been used to describe ac-induced enhancement of the low-field dc conductivity in $NbSe_3$ and TaS_3 , and there provides excellent quantitative fits.^{11,13} We assume a form

$$\Delta Y/Y = c_2 X_0 \quad (8)$$

with c_2 a normalization constant. Equation (8) provides a good fit to the data of Fig. 5. The solid line in Fig. 5 is Eq. (8), with fitting parameters $\omega_0^2\tau = 0.4$ MHz and $c_2 eE_{ac}/m^* \omega_0^2 = -4 \times 10^{-3}$. On the other hand, the value used for the “crossover” frequency $\omega_0^2\tau$ is unrealistically small in light of ac conductivity experiments³² on TaS_3 which show $\omega_0^2\tau \approx 900$ MHz. We thus rule out simple rigid particle displacement as being the sole origin of the ac-induced lattice softening.

Ac conductivity provides an independent probe of averaged CDW displacement. Even for $E_{ac} \ll E_T$, the CDW electronic response in TaS_3 and $NbSe_3$ is highly nonlinear. Stokes *et al.*³³ have demonstrated a highly E_{ac} - and ω_{ex} -dependent complex dielectric function ϵ in TaS_3 in the frequency range $\omega_{ex}/2\pi = 3$ KHz to 1 MHz. They find a dielectric constant which, with increasing E_{ac} , deviates

markedly from its $E_{ac} \rightarrow 0$ value, the deviation being more severe at lower frequency. This behavior is analogous to the elastic data of Fig. 5. Stokes *et al.* conclude that the E_{ac} dependence of ϵ is inconsistent with rigid motion of the CDW condensate, and suggest a distribution of pinning fields; such a distribution introduces new degrees of freedom. A direct comparison between $Y(E_{ac})$ and $\epsilon(E_{ac})$ is complicated by the fact that the electronic response is highly nonlinear for $E_{ac} \rightarrow E_T$. For a sinusoidal electric field excitation, a nonsinusoidal response follows, and only the Fourier component of the response at ω_{ex} contributes to ϵ . In the elastic measurements, on the other hand, all Fourier components of the electronic response may couple into ΔY , which is measured mechanically in the limit of linear mechanical response.

The coupled Eqs. 6(a) and 6(b), which take both CDW and lattice elasticity into account, predict²⁹ a decrease in Y with increasing E_{ac} , even with $E_{ac} \ll E_T$. This is a direct result of the multiple degrees of freedom of the CDW condensate (parametrized by k_c) in the model, which again suggests an important role played by CDW incoherence in the elastic properties of a CDW crystal.

Independent of any particular model, the sharp anomaly in the $\Delta Y/Y$ behavior of Fig. 6 as $\omega_{ex} \rightarrow 0$ is suggestive of critical behavior. If we assume a form

$$\Delta Y/Y = C(\omega_{ex}/2\pi - \omega_{cr}/2\pi)^{-\alpha}, \quad (9)$$

with C a constant, then the dashed line of Fig. 6 may again be fit with $\alpha = 0.867$ and $C = 108$ (assuming $\omega_c \ll \omega_{ex}$). From the limited data points of Fig. 6 the value of ω_{cr} cannot be determined.

B. Finite E_{ac} , finite E_{dc}

In the presence of dc electric fields E_{dc} alone, Y and δ in TaS_3 and $NbSe_3$ are unaffected by the dc field until E_{dc} exceeds E_T . Figure 7 demonstrates that the same holds true also in the presence of an additionally applied ac field E_{ac} . In effect, the lattice softening and increase in internal friction generated by E_{ac} (with $E_{dc} = 0$) define new effective “pinned” values for Y and δ . Deviations in Y and δ from the pinned values are apparently first observed at $E_{dc} = E_T'$, the dc threshold field measured in the presence of the ac field.

The reduction of E_T with increasing E_{ac} has been previously discussed for $NbSe_3$ and TaS_3 from an electronic transport point of view. The conductivity observations are consistent with Eq. (4), the simple rigid particle description, or a quantum tunneling mechanism.^{11–14} In the analysis of the electronic behavior, it is generally assumed that the magnitude of the periodic pinning potential is unaffected by E_{ac} ; the ac field simply helps the CDW overcome the fixed pinning potential barrier, leading to enhanced dc conductivity. Since pinning of the CDW involves CDW phase fluctuations and the underlying lattice structure (containing the impurity atoms), the question naturally arises if the reduction in E_T due to E_{ac} may in fact be due solely to the softening of the lattice elasticity. A careful comparison between Fig. 8 (which shows I_T' versus E_{ac}) and Fig. 3 (which shows Y versus

E_{ac}) indicates that there exists no simple relationship between I'_T and Y : for small E_{ac} , $\Delta Y/Y$ vanishes asymptotically as $E_{ac} \rightarrow 0$, while I'_T decreases linearly with increasing E_{ac} for small ac excitations. A similar lack of direct correspondence between Y and E_T is found in the temperature dependences of those parameters in NbSe_3 and TaS_3 (measured with $E_{ac}=0$).

A constant local pinning potential barrier is assumed also in Eqs. 6(a) and 6(b). The predicted reduction in E_T with increasing E_{ac} in that model is very similar to that associated with rigid particle behavior.¹¹ The corresponding elastic properties predicted²⁹ by Eqs. 6(a) and 6(b) demonstrate breaks in Y and δ as functions of E_{dc} which correspond precisely to E'_T , the threshold field for CDW depinning. This is consistent with experiment and is a consequence of the assumption $Y = Y_L + Y_C$.

In the discussion of original elasticity experiments on TaS_3 in the presence of dc electric fields, it was suggested⁴ that the functional forms of Y and δ may be directly related to the CDW drift velocity v_d . The data of Figs. 10 and 12, which shows the elastic properties during Shapiro step electronic interference, demonstrates that this is clearly not the case for TaS_3 or NbSe_3 . During Shapiro step interference, a portion (macroscopic domain) of the CDW condensate becomes mode locked to the external ac drive, effectively fixing the CDW drift velocity of that domain at $v_d = J_{CDW}/n_c e = \lambda(p/q)\omega_{ex}/2\pi$, with λ the CDW wavelength. J_{CDW} is the excess current carried by the CDW through the macroscopic domain. If Y and δ were strictly functions of v_d , then mode locking would result in regions of constancy in the Y and δ versus I_{dc} curves, in sharp contrast to the strong peak anomalies observed in Fig. 10 for TaS_3 and in Fig. 12 for NbSe_3 .

As mentioned previously, during mode locking the behavior of Y and δ is to tend toward the value characteristic of the pinned, $I_{dc}=0$ state; the same holds true for dV/dI . In general, in a dV/dI interference experiment the interference peaks do not attain the ohmic value. Consequently the height h of the dV/dI peak (measured from the effective baseline, neglecting the peak structure) is only a fraction of the maximum possible peak height³⁴

$$h_{max} = [(dV/dI)_{I_{dc}=0}] - [(dV/dI)_{unlocked}] .$$

This is clearly observed in Fig. 12(b) for NbSe_3 , where the $n=1/1$ interference peak in dV/dI has $h/h_{max}=0.75$, suggesting that the locked domain comprises 75% of the sample volume, while for the $n=1/2$ peak $h/h_{max}=0.25$, suggesting that the locked domain comprises 25% of the sample volume for this interference. As seen in the Y and δ traces in the same figure, the corresponding peak anomalies in Y and δ show nearly identical scaling. For example, the $n=1/1$ interference peak corresponds to an anomaly in Y which reaches (correcting for the sloping baseline) approximately 75% of the $I_{dc}=0$ value; the same holds true for the $n=1/1$ anomaly in δ . Similar 25% peak heights are observed in Y and δ during the $n=1/2$ interference. This suggests that a fully mode-locked CDW, with $h/h_{max}=1$, would display elastic constants indistinguishable from the pinned, $I_{dc}=0$ state.

On the other hand, the data of Fig. 10(b), appropriate to TaS_3 , shows a rough but inexact scaling between the

anomalies in dV/dI , Y , and δ . In particular, the *smaller* dV/dI peak at $I_{dc}=64 \mu\text{A}$ is associated with the *larger* peak anomalies in Y and δ . This suggests that the mode-locked region associated with this interference peak might be physically located near the clamped region of the crystal, where small changes in local elastic constants have a strong influence on the elastic properties determined for the overall crystal.

The behavior of Y and δ during electronic mode locking suggests that Y_L and Y_C again couple strongly during mode lock and $Y = Y_L + Y_C$. This is not an obvious result, since during mode lock the CDW dynamics are determined primarily by the external ac field. Hence one might expect that Y_L and Y_C fully *decouple* during mode lock, yielding $Y = Y_L$. The experimental results show this to not be the case, and argue strongly that internal degrees of freedom of the CDW condensate are central to the elastic anomalies. Although the behavior of Y and δ during mode locking has not been investigated in the framework of anelastic relaxation models, it is apparent that if the functional forms of Y and δ versus E_{dc} are the direct result of CDW incoherence, then an increase in CDW coherence, such as that resulting from electronic mode locking, will lead to peak structure in Y and δ during mode lock.

CDW incoherence arising from CDW internal modes is central to Eqs. 6(a) and 6(b), which predict electronic mode locking in the presence of combined dc and ac electric fields. The model also predicts corresponding sharp peak anomalies in Y and δ in excellent agreement with experiment. Figure 13 shows an analog computer solution²⁹ of Eqs. 6(a) and 6(b) for dV/dI , Y , and δ , for an ac drive field $E_{ac}/E_T = 5$ and with $\omega_{ex}/\omega_0^2\tau = 0.05$. It is apparent that, during electronic mode locking, Y and δ tend toward their pinned, $I_{dc}=0$ values, consistent with the experimental results of Figs. 10(b) and 12(b). In the model, the behaviors of Y and δ during mode lock

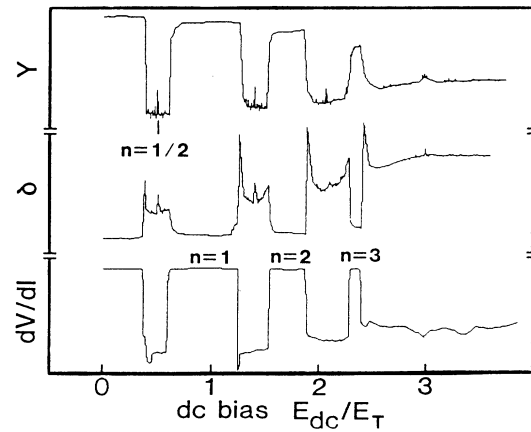


FIG. 13. Y , δ , and dV/dI as calculated from a many-degree-of-freedom model [Eqs. 6(a) and 6(b)]. Interference structure is observed analogous to that found experimentally in TaS_3 and NbSe_3 (Figs. 10 and 12). The calculated curves are from Ref. 29.

reflects a reduction in effective internal degrees of freedom; the CDW phason couples strongly to the underlying phonon structure, and $Y = Y_L + Y_C$.

A reduction in internal degrees of freedom during electronic mode locking has been observed in other CDW transport measurements, in particular the broad-band noise. During complete ($h/h_{\max} = 1$) mode locking, broad-band noise generated by a moving CDW is fully eliminated.¹⁷ Since the source of the broad-band noise may be interpreted as arising from CDW incoherence, the vanishing of the noise is evidence for a "freeze out" of effective internal degrees of freedom during mode locking. Hence there may exist a fundamental correspondence between the broad-band noise and the elastic properties of CDW conductors. We note also that the decrease in δ caused by an ac field in the sliding CDW state of TaS₃ at 115 K (Fig. 9) could be the result of ac-induced coherence between CDW domains. Strong ac fields applied to CDW conductors result in enhanced CDW electronic phase homogenization, as evidenced by the suppression of broad-band noise by large amplitude ac fields,¹⁷ the independence of Shapiro step quality on the narrow-band noise spectrum,¹⁶ and an increased resistance to splitting of mode-locked regions in the presence of temperature gradients.³⁵ An analogous elastic process in a conventional metal is the substantially greater (at certain frequencies and temperatures) internal friction δ for a polycrystalline specimen than for a single crystal specimen; this results from relaxation of domain boundaries under stress.³⁶ In TaS₃, the narrow-band noise spectrum becomes extremely complex as the temperature is lowered,³⁷ signifying increased disorder and generation of multiple current domains at lower temperatures. This may explain why δ decreases dramatically with increasing ac field amplitude in TaS₃ at low temperatures, as demonstrated for the region $I_{dc}/I_T > 2$ in Fig. 9.

IV. CONCLUSION

Measurement of the elastic properties of TaS₃ and NbSe₃ in the presence of ac and combined ac and dc electric fields has revealed important results complementary to those previously obtained in the limit of dc fields alone. Lattice softening in the presence of ac fields with $E_{ac} < E_T$ demonstrates that the CDW need not be depinned in the Fröhlich sliding mode sense to achieve a decrease in Y , but need only be in motion on a local scale. The behavior of Y and δ on electronically mode-locked steps demonstrates that the CDW drift velocity alone does not dictate elastic properties in the sliding state, and that an absolutely essential role is played by the internal degrees of freedom of the CDW condensate. The assumption that $Y = Y_L + Y_C$ in the pinned and mode-locked states, and $Y = Y_L$ in the sliding state, appears valid.

The strong correspondence between the elastic and electronic properties of CDW conductors has important implications for the interpretation of previously obtained electronic response parameters.¹ It is also apparent that any complete model of CDW electronic response must incorporate in a fundamental way coupling of the deformable CDW (obeying classical or quantum dynamics) to the deformable lattice.

ACKNOWLEDGMENTS

We thank Professor J. Brill, Professor L. M. Falicov, Dr. S. Coppersmith, and M. S. Sherwin for illuminating discussions. This research was supported by National Science Foundation (NSF) grant No. DMR-84-00041. AZ also acknowledges support from the Alfred P. Sloan Foundation and the IBM Corporation.

¹For recent reviews, see G. Grüner and A. Zettl, *Phys. Rep.* **119**, 117 (1985); *Electronic Properties of Inorganic Quasi-One-Dimensional Materials*, edited by P. Monceau, (Reidel, Dordrecht, 1985), Vols. 1 and 2; *Charge Density Waves in Solids*, edited by Gy. Hutiray and J. Solyom (Springer, New York, 1985).

²M. Barmatz, L. R. Testardi, and F. J. DiSalvo, *Phys. Rev. B* **12**, 4367 (1975).

³L. R. Testardi, *Phys. Rev. B* **12**, 3849 (1975).

⁴J. W. Brill and W. Roark, *Phys. Rev. Lett.* **53**, 846 (1984).

⁵G. Mozurkewich, P. M. Chaikin, W. G. Clark, and G. Grüner, in *Charge Density Waves in Solids*, edited by Gy. Hutiray and J. Solyom (Springer, New York, 1985), p. 353; G. Mozurkewich, P. M. Chaikin, W. G. Clark, and G. Grüner, *Solid State Commun.* **56**, 421 (1985).

⁶J. W. Brill, W. Roark, and G. Minton, *Phys. Rev. B* **33**, 6831 (1986).

⁷M. H. Jericho and A. M. Simpson, *Phys. Rev. B* **34**, 1116 (1986).

⁸L. C. Bourne, M. S. Sherwin, and A. Zettl, *Phys. Rev. Lett.* **56**, 1952 (1986).

⁹J. T. Tiedje, R. R. Haering, and W. N. Hardy, *J. Acoust. Soc.*

Am. **65**, 1171 (1979).

¹⁰P. Morse, *Vibration and Sound*, 2nd ed. (McGraw-Hill, New York, 1948); see also J. T. Tiedje, Ph. D. thesis, University of British Columbia, 1977 (unpublished).

¹¹G. Grüner, W. G. Clark, and A. M. Portis, *Phys. Rev. B* **24**, 3641 (1981).

¹²A. Zettl and G. Grüner, *Phys. Rev. B* **29**, 755 (1984).

¹³G. Grüner and A. Zettl, *Phys. Rep.* **119**, 117 (1985).

¹⁴J. R. Tucker, J. H. Miller, Jr., K. Seeger, and J. Bardeen, *Phys. Rev. B* **25**, 2979 (1982); R. E. Thorne, W. G. Lyons, J. W. Lyding, J. R. Tucker, and John Bardeen, *Phys. Rev. B* **35**, 6348 (1987) **35**, 6360 (1987).

¹⁵A. Zettl, and G. Grüner, *Solid State Commun.* **46**, 501 (1983).

¹⁶R. P. Hall and A. Zettl, *Phys. Rev. B* **30**, 2279 (1984).

¹⁷M. S. Sherwin and A. Zettl, *Phys. Rev. B* **32**, 5536 (1985).

¹⁸J. Bardeen, *Phys. Rev. Lett.* **45**, 1978 (1980).

¹⁹L. Sneddon, M. C. Cross, and D. S. Fisher, *Phys. Rev. Lett.* **49**, 292 (1982).

²⁰L. Sneddon *Phys. Rev. B* **29**, 719 (1984); **29**, 725 (1984); *Phys. Rev. Lett.* **52**, 65 (1984).

²¹P. B. Littlewood, *Phys. Rev. B* **33**, 6694 (1986).

²²G. Grüner, A. Zawadowski, and P. M. Chaikin, *Phys. Rev.*

- Lett. **46**, 511 (1981).
- ²³A. J. Berlinsky, Rep. Prog. Phys. **42**, 1243 (1979).
- ²⁴See, for example, H. Fukuyama and H. Takayama, in *Electronic Properties of Inorganic Quasi-One-Dimensional Materials*, edited by P. Monceau (Reidel, Dordrecht, 1985), Vol. 1. p. 41.
- ²⁵S. N. Coppersmith and C. M. Varma, Phys. Rev. B **30**, 3566 (1984).
- ²⁶P. A. Lee and T. M. Rice, Phys. Rev. B **19**, 3970 (1979).
- ²⁷H. Fukuyama and P. A. Lee, Phys. Rev. B **17**, 535 (1978).
- ²⁸P. B. Littlewood (unpublished).
- ²⁹M. S. Sherwin and A. Zettl (unpublished); M. S. Sherwin and A. Zettl, Physica D **23**, 62 (1986).
- ³⁰L. Sneddon, Phys. Rev. Lett. **56** 1194 (1986).
- ³¹Of course, with finite $E_{dc} < E_T$ the CDW becomes polarized, and hence there is a finite *static* displacement from true “equilibrium.” However, curve *A* in Fig. 2 (see also Refs. 4–6) shows that both Y and δ are insensitive to dc CDW polarization as long as $E_{dc} < E_T$. In other words, the elastic properties of a static CDW are insensitive to local metastable-state configurations.
- ³²S. Shridar, D. Reagor, and G. Grüner, Phys. Rev. Lett. **55**, 1196 (1985).
- ³³J. P. Stokes, M. O. Robbins, and S. Bhattacharya, Phys. Rev. B **32**, 6939 (1985).
- ³⁴A. Zettl, Physica D **23**, 155 (1986).
- ³⁵M. F. Hundley and A. Zettl, Phys. Rev. B **33**, 2883 (1986).
- ³⁶A. S. Nowick and B. S. Berry, *Anelastic Relaxation in Crystalline Solids* (Academic, New York, 1972), p. 439.
- ³⁷A. Zettl and G. Grüner, Phys. Rev. B **28**, 2091 (1983).